Volume 14, Issue 1 (2026) pp. 48-71 **DOI**: 10.48309/IJABBR.2026.2063133.1619

Original Article

Characterization and Performance Evaluation of Silk Fibroin/Polylactic Acid Composite Nanofiber Scaffolds for Tissue Engineering and Wound Healing

Maede Afzali[1, 2] | Mahboubeh Mirhosseini[1,*] | Habib Nikukar[3,4*] | Hosein Molla Hoseini[5] | Fatemeh Sadeghian-Nodoushan[3,4] | Fahime Mazaheri [3,4] | Mojgan Moshrefi [3,4]

[1]Department of Biology, Faculty of Science, Payame Noor University, Tehran, Iran

[2]Department of Tissue Engineering, School of Advanced Technologies in Medicine, Tehran University of Medical Sciences, Tehran, Iran

[3]Biotechnology Research Center, Yazd Reproductive Sciences Institute, Shahid Sadoughi University of Medical Sciences, Yazd, Iran

[4]School of Advanced Medical Sciences and Technologies, Shahid Sadoughi University of Medical Sciences, Yazd, I. R. Iran

[5]District 1, Yazd education and training organization, Yazd, Iran

*Corresponding Author E-mail: m.mirhosseini@pnu.ac.ir ; habibnik@ssu.ac.ir

Submitted: 2025-06-09, Revised: 2025-08-03, Accepted: 2025-09-07

Abstract

Nanofiber scaffolds constructed from both natural and synthetic polymers represent highly advantageous materials within the domains of tissue engineering and regenerative medicine. Combining silk fibroin (SF) with poly (lactic acid) (PLA) can potentially enhance biocompatibility, mechanical properties, and wound healing capabilities, making these composites suitable for skin regeneration applications. This study investigated composite nanofibers made from varying ratios of SF and PLA, using electrospinning techniques. The scaffolds were characterized using scanning electron microscopy (SEM) and Fourier-transform infrared (FTIR) spectroscopy to elucidate their morphological characteristics and chemical composition. Methanol management was employed to modify crystallinity. Wettability was assessed via water contact angle measurements. Biological behavior was evaluated using fibroblast adhesion, spreading, and proliferation assays. SEM was also used to observe cell morphology and filopodia formation. Macroscopic and histological analyses assessed skin wound healing *in vivo* SEM images demonstrated uniform nanofibers without beads, and FTIR confirmed successful fabrication with changes in crystallinity after methanol treatment. Higher SF content reduced the water contact angle, indicating increased hydrophilicity. Fibroblasts showed enhanced adhesion, spreading, and proliferation on SF/PLA-70/30 scaffolds, especially after methanol treatment, with increased filopodia indicating better attachment. *In vivo* studies revealed that scaffolds with higher PLA content (SF/PLA-30/70 and SF/PLA-50/50) significantly accelerated skin wound healing and tissue regeneration. The combination of SF and PLA in nanofiber scaffolds improves cell attachment, proliferation, and skin healing, demonstrating their potential in tissue engineering. This study highlights the promising application of SF/PLA composites for skin regeneration and regenerative medicine, emphasizing their role in enhancing wound repair processes.

Keywords: Biomaterials, Human fibroblasts, Scaffolds, *In vivo* experiments, Electrospinning techniques, Regenerative medicine.

Introduction

Tissue Engineering (TE) and wound healing are fast-developing areas in medical research, that concentrate on new tissue regeneration methods [1]. These strategies have drawn attention due to their three-dimensional framework, similar to the extracellular matrix (ECM), supporting major cell functions, example such as attachment, proliferation, and differentiation [1-3]. Among the most promising materials for scaffold fabrication are silk fibroin (SF) and poly (lactic acid) (PLA) due to their unique properties and biocompatibility. SF is a protein from the silk threads of silkworms, noted for its mechanical properties, biodegradability, and biocompatibility [4]. SF scaffolds stimulate cell adhesion, growth, and differentiation, construction them suitable for TE purposes [5]. PLA is a biodegradable synthetic polymer that is in extensive use in TE applications due to its strength and biodegradability. PLA scaffolds retain their integrity and can be fabricated precisely to control their characteristics [4]. This allows for the construction of scaffolds with precise structures for specific tissue needs. Newly, composite scaffolds made from SF and PLA have been widely studied for their synergistic benefits. Blending SF with PLA may enhance mechanical strength, hydrophilicity, and cell adhesion and proliferation [4,6]. SF can actively contribute to the composite scaffold, signaling cells for tissue regeneration and wound healing. Its incorporation in PLA scaffolds enhances cell signaling, supports matrix deposition, and promotes vascularization to speed up healing [3,6]. The composite structure of SF and PLA scaffolds allows the optimization of scaffold traits by adjusting the material ratio and arrangement. This flexibility lets researchers customize scaffold properties to meet specific tissue or wound healing needs [6]. This investigation aims to assess the SF/PLA composite nanofiber scaffold for tissue engineering and wound healing. The scaffolds were made by electrospinning, which generates nanofibers with a large surface area-to-volume ratio and tunable characteristics. Nanofiber scaffolds have been characterized by SEM, FTIR, and water contact angle measurements for morphology, composition, crystallinity, hydrophilicity, and wettability. Their fabrication technique, electrospinning, allows the creation of a great variety in the type and properties of nanofibers, with a large surface area-to-volume ratio and tunable characteristics. The biotic operation of the SF/PLA merged nanofiber scaffolds was assessed by cell proliferation, adhesion, and skin healing. Fibroblasts, important for wound healing, were cultured on the scaffolds to determine their capability to maintain cell growth and attachment [2]. Macro and microscopical analyses were performed to evaluate the scaffolds' ability in skin healing *in vivo*. These results help to understand the SF/PLA composite nanofiber scaffolds for TE and wound healing. Improved biomaterials are essential for tissue regeneration;therefore, SF/PLA scaffolds show great promise in this field.

Materials and Methods

Materials

PLA, with a molecular weight of 90 kDa used in the current study bought from Zhejiang Hisun Biomaterials Co., Ltd., Taizhou, China. The raw silk fibers used in this work were provided by Lahijan, province of Gilan, Iran. The 3-(4,5-dimethyl-2-thiazolyl)-2,5-diphenyl-2H-tetrazolium bromide (MTT), employed in the experimental work, was obtained from Sigma–Aldrich ® Inc., St.

Louis, Missouri, United States. Cell culture media, such as DMEM, FBS, trypsin-EDTA, PBS, RPMI 1640 powder, and antibiotics, were all provided by Gibco ® of Life Technologies, Germany. Trifluoroacetic acid (TFA), methanol, glutaraldehyde, and all other materials used were purchased from Merck ® Company. Human foreskin fibroblast (hFF, Batch 18) was provided by the Biotechnology Research Center at Shahid Sadoughi University, Yazd, Iran.

Preparation of Silk Fibroin Powder

During the initial degumming process, raw silk fibers underwent two treatments with a 0.5% (w/v) sodium carbonate solution at 100 °C for 30 min, and were then rinsed three times with distilled water. After that, the degummed silk was dissolved in a ternary solvent system, $CaCl_2/CH_3CH_2OH/H_2O$ (molar ratio 1:2:8), at 70 °C for 2 h to obtain a clear solution. The final SF solution was filtered through an 80-mesh polyester mesh and subsequently filtered through a 0.2 µm syringe filter to eliminate any residual large particles. Afterward, the SF solution was subjected to dialysis in distilled water at room temperature for three days using a cellulose tubular membrane with a 12 kD molecular weight cut-off, with the water being changed every 2 h. The process yielded SF sponges, which were subsequently allowed to dry at ambient temperature for 72 h.

Electrospinning

PLA and SF were separately dissolved in TFA solvent at 12% (w/v) and stirred for 4 h. The suspensions were transferred into syringes with a 21 G needle and loaded into an electrospinning setup (Lab Electroris, Fanavaran Nano Meghyas Co, Iran).

In electrospinning, the collector drum, placed 18 cm from the syringe pump, was wrapped with aluminum foil and supplied with 18 kV at a flow rate of 0.1 ml/h [7]. Spinning parameters were optimized for PLA, SF, and SF/PLA composite nanofibers at ratios of 70:30, 50:50, and 30:70.

Surface Modification of Nanofibrous Scaffolds

Methanol treatment was applied to certain nanofiber compositions to stimulate β-sheet formation in SF, rendering it insoluble. They were dipped in 90% methanol for 60 seconds, washed, and then air-dried under vacuum for a day to remove moisture [8].

Characterization of nanofibers

SEM

The electrospun nanofibers were cut to approximately 1 × 1 cm and gold-coated by a desk sputter coater (DSR1, Nano-structured Coatings, Iran). After that, they were analyzed with the SEM (Phenom ProX Desktop SEM-Thermo Fisher Scientific®, USA) to view their surface morphology. To calculate the mean fiber diameter and standard deviation, 100 fibers were randomly selected using ImageJ® software (Version 1.46). The pore surface area from SEM images was calculated with ImageJ, converted into a round part, and the round diameter was used as the pore diameter.

FTIR

Chemical analysis of scaffolds was carried out in FTIR spectroscopy (Hartmann & Braun ®, Canada) using KBr method. It covered the series of the spectrum between 4000 and 400 cm^{-1}. To determine structural characteristics of scaffolds, the FTIR spectra obtained were

compared and analyzed using OriginPro ® software (Version 94E).

Biodegradability Evaluations

The water absorption ratio and biodegradation characteristics of the nanofiber scaffolds were evaluated by immersion in 5 ml of PBS solution (pH 7.4) for predetermined periods of 2, 4, 6, 24, 48, and 72 h under dynamic conditions at 37 °C and a stirring rate of 60 rpm in a 15 ml tube. At the end of each programmed time interval, the specimens were separated from the PBS solution and immediately assessed, having carefully removed the excess external moisture with filter paper. Thereafter, the water absorption was calculated by the following formula:

$$\text{Water uptake (\%)} = [(MW_t - MW_0) / MW_0] * 100 \quad (1)$$

Where, MW_0 denotes the specimen's original weight prior to immersion, while MW_t indicates its wet weight at a specific time point (t) after removal from the PBS.

For assessing water uptake, the samples were rinsed with distilled water and dried in an oven at 60 °C for 2 h. The weight loss was then calculated using the following formula:

$$\text{Weight loss (\%)} = [(Md_0 - Md_t) / Md_0] * 100 \quad (2)$$

Md_0, represents the dry weight of the specimen at time 0, while Mdt, represents of the specimen at time t after immersion and drying at 60 °C until a stable weight is achieved.

Contact Angle Test

The hydrophilicity and water adsorption properties of the various scaffolds have been determined using water contact angle measurements with goniometry as well as Digimizer software version 4.6.1. In the case of all the electrospun scaffolds, a 10 µl droplet was automatically dispensed to apply distilled water three times from different locations on the scaffold before and after treatment with methanol. A digital microscope (MV500, China) captured images at 3 and 10 seconds, which were subsequently analyzed [9].

Mechanical Properties

The tensile strength of the nanofibrous mats was measured using a universal tensile testing machine, Micro-350 (Sherli, UK), equipped with a high-resolution load cell capable of measuring loads of up to 50 N. The test was performed at a speed of 10 mm/min. The nanofibers were initially shaped into rectangular samples measuring 20 mm in width and 10 mm in height, with a thickness ranging from 100 to 150 µm. The sample's thickness was measured by a micrometer [10].

Biocompatibility Evaluation

Cell Seeding

The human foreskin fibroblast (hFF) was cultured using a standard cell culture medium made of DMEM, 10% FBS, and 100 units/ml of antibiotics. The cells were cultured in a 25 cm^2 cell culture bottle and maintained in a standard cell culture incubator at 37 °C with a 5% CO_2 atmosphere. The culture was changed every two days to maintain optimal cell conditions. For the experiment, sterilized coverslips with electrospun nanofiber scaffolds were placed in each well of a 24-well plate. They were UV-treated for 1 h and washed three times with PBS buffer to maintain sterility. When the cells reached 80% confluency, they were detached with 0.025% trypsin-EDTA, counted, and seeded at 10,000 cells/well onto the scaffolds in 400 µl per well, fully wetting

the fibers. The culture was changed every three days to provide nutrients and maintain cell viability.

Cell Culture Study

After 1, 3, and 7 days of cell culture, the cellular scaffolds were rinsed in PBS twice to remove any unattached cells. The scaffolds were manipulated in 2.5% phosphate-buffered glutaraldehyde at 4 °C for 2 h. Consequently, the specimens were desiccated in ambient air for a duration of one night and subsequently exposed to staining with hematoxylin and eosin (H&E) for the purpose of histological examination. To analyze, segments of the H&E-stained samples were viewed using an optical microscope (BA310E, Olympus, Japan). The fixation of the cellular scaffolds was achieved by progressive dehydration using ethanol at concentrations of 70%, 96%, and 100%; each concentration was used for 5 minutes. Following the process of dehydration, the scaffolds underwent sputter-coating with gold in preparation for scanning electron microscopy (SEM) imaging after a duration of three days.

Cell Proliferation Study

After seven days, the proliferation of cells on nanofiber scaffolds was evaluated using the MTT assay. At specified time intervals, a solution containing 5 mg/ml of mitochondrial reagent in phenol red-free RPMI 1640 (10% v/v) was introduced into each well and incubated in a dark environment for 4 h. After the incubation, the culture medium was removed via aspiration, and the dye was stabilized overnight using acidic isopropanol (0.04–0.1 N HCl in absolute isopropanol). The resulting mixture was then dispensed into 96-well plates for further analysis. The outcomes were quantified using an ELISA microplate reader (Fluostar Optima, BMG Lab Technologies, Germany) at a wavelength of 570 nm, with background signals being subtracted at 630 nm.

Wound Healing in Wistar Rats

Wound healing of methanol-treated scaffolds was studied using Wistar rats from Shahid Sadoughi University, Yazd, Iran. Adult male rats, 180-250 g in weight, were kept in single polycarbonate cages in standard conditions: 25 ± 2 °C with 60-70% humidity and a 12 h light-dark cycle. Animals were fed a pellet diet and provided with water for one week before the experiment. All methods were authorized by the Research Ethics Committee and followed Shahid Sadoughi University guidelines (ethics code: IR.SSU.REC.1395.243).

Rats were anesthetized by intraperitoneal injection of ketamine-xylazine hydrochloride (50 and 10 mg/kg of body weight, respectively). Afterward, the dorsal fur was shaved and cleaned with Betadine (Povidone-iodine). Two square excisional sites, each 10 ± 0.2 mm^2, were created on their backs. The rats were divided into five groups. The left wounds were identified as a, b, c, d, and e for methanol treatments of SF, SF/PLA (70:30), SF/PLA (50:50), SF/PLA (30:70), and PLA. The right wounds were used as a negative control, cleaned only with physiological serum. Macroscopic photos measured the wound area on days 0, 9, and 18 post-wound induction. Wound closure percentage was analyzed as:

$$\text{Wound closure (\%)} = (A_0 - A_t) / A0 * 100 \quad (3)$$

Where, A_0 represents the wound area on day 0, while at denotes the wound area at time t. Healing parameters included re-epithelialization, dermal cellularity, granulation tissue formation, angiogenesis, and skin appendages development. Wound areas and nearby

tissues were erased on days 9 and 18, manipulated in 10% buffered formalin, and processed for histopathology. Samples were blocked in paraffin, segmented to 5 µm with a microtome, and stained with H&E for microscopy [11].

Statistical Analysis

The values were calculated as means ± standard deviation (SD) and presented as averages. Statistical differences were analyzed using one-way ANOVA with the SPSS software package (SPSS software, Version 24.0, USA). Statistical significance was considered at *p-value < 0.05 (n = 3).

Results

Characterization of Nanofibers

Morphology of Nanofibers

Figure 1 displays the SEM images of different nanofibers. The 12% concentration fibers have a smooth surface with no beads. Table 1 lists the average diameter and pore size of the nanofibers pre- and post-methanol treatment. The diameters of the electrospun nanofibers range from 150 nm to 194 nm, with SF being the smallest and PLA the largest. Rising PLA concentration leads to larger fiber diameters. The average pore size is estimated to be about 444 nm to 485 nm, as listed in Table 1. Methanol treatment significantly increases the mean diameter of SF and SF/PLA nanofiber scaffolds compared to that of PLA, leading to a sharp decrease in the average pore size.

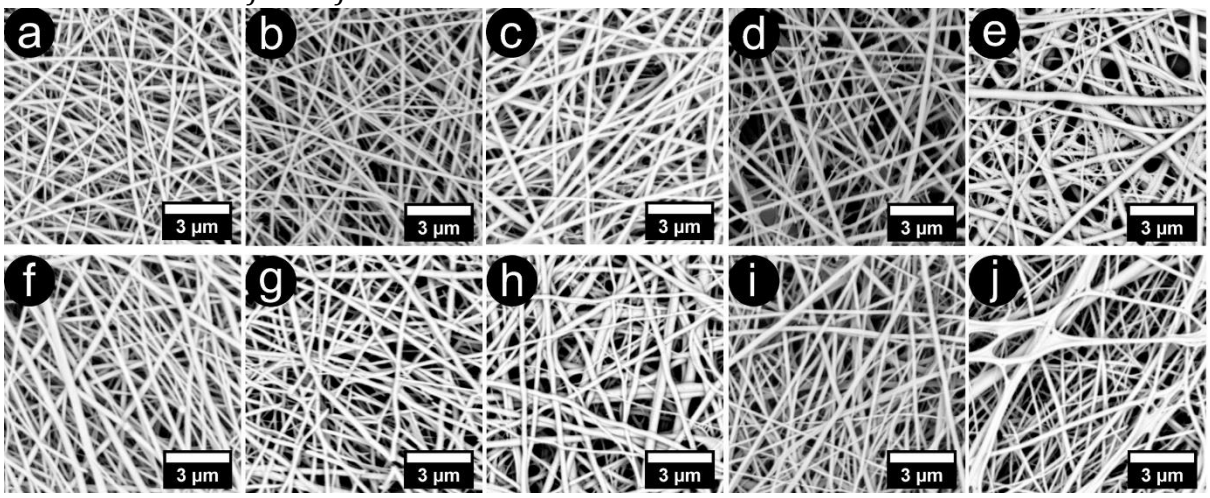

Figure 1 SEM pictures of nanofiber scaffolds with different composite ratios without methanol treatment: (a) SF, (b) SF/PLA (70:30), (c) SF/PLA (50:50), (d) SF/PLA (30:70), (e) PLA; and with methanol treatment: (f) SF, (g) SF/PLA (70:30), (h) SF/PLA (50:50), (i) SF/PLA (30:70), and (j) PLA (scale bar: 3 µm= 3000 nm)

Table 1 The mean diameter and surface pore size of the nanofiber scaffolds before and after methanol treatment (n=100)

Substrate	Untreated		Methanol-treated	
	Diameter (nm)	Pore size (nm)	Diameter (nm)	Pore size (nm)
SF	150±64	444±183	191±71	430±199
SF/PLA-(70:30)	151±47	453±187	190±59	445±192
SF/PLA-(50:50)	167±52	471±178	187±60	466±185
SF/PLA-(30:70)	178±77	480±199	186±65	476±164
PLA	194±73	485±154	184±75	487±98

Nanofibers Structure

The FTIR spectrum of the untreated fibroin nanofibers (Figure 2(f)) exhibited intense absorption bands at 1654 cm^{-1} (corresponding to amide I, CO, and CN stretching), 1542 cm^{-1}, and 1238 cm^{-1} (corresponding to amide II and III, respectively, NH bending and CN stretching), and a band at 674 cm^{-1} (corresponding to amide V, CN torsion, and NH bending). The results obtained from FTIR analysis revealed that PLA showed characteristic bands at 864 cm^{-1} (C-C peaks), 2996 cm^{-1} (C-CH_3 groups), 1760 cm^{-1} (carbonyl (C=O) groups), 1456 cm^{-1} (CH(CH_3) groups), 1364 cm^{-1} (CH_3 groups), and 1183 cm^{-1} (O-C-O groups). Moreover, three peaks were observed at 1129, 1090, and 1046 cm^{-1}, which correspond to C-C-O groups (Figure 2(b)). The spectral analysis of the SF/PLA composite in a 50/50 ratio (Figure 2(d)) revealed absorption peaks characteristic of both fibroin and polylactic acid, thereby justifying the formation of composite nanofibers. Subsequently, the result of methanol action on the crystallinity of pure and composite nanofibers was analyzed. The FTIR spectroscopy analysis for the treated fibroin nanofibers (Figure 2(e)) showed prominent bands at 1631, 1523, and 1232 cm^{-1}. In contrast, the structure of PLA nanofibers showed little change after methanol treatment (Figure 2(a)). The treatment of methanol on electrospun SF/PLA at a 50/50 ratio resulted in a shift in the position of the N-H bending vibration bond (amide II) from 1541 to 1520 cm^{-1}, compared to untreated SF/PLA and the SF blend (Figure 2(c)). While methanol treatment did not induce amide peaks in the protein's FTIR spectrum, it did result in peak shifts. The spectra showed absorption bands of silk fibroin at 1654, 1542, and 1238 cm^{-1}, which are assigned to random coil and silk I (α-form) structures. However, after methanol treatment, amide I, II, and III bands were shifted to 1631, 1523, and 1232 cm^{-1}, respectively, which correspond to silk II (β-form) conformation [12]. These findings suggest that methanol treatment altered the secondary structure of silk fibroin from α-helix/random coil to β-sheet [8] .

Biodegradation Behavior of the Nanofibers

In this research, the water swelling behavior of untreated and methanol-treated nanofibers was studied in PBS at pH 7 for 2, 4, 6, 24, 48, and 72 h. Based on Figure 3(a), untreated SF/PLA-70:30 nanofibers had good water absorption, and the maximum water intake was achieved after 72 h of soaking time.

Alternatively, untreated PLA nanofibers exhibited the lowest water uptake within the PBS solution. Untreated and methanol-treated SF nanofibers increased the water content in the matrix.

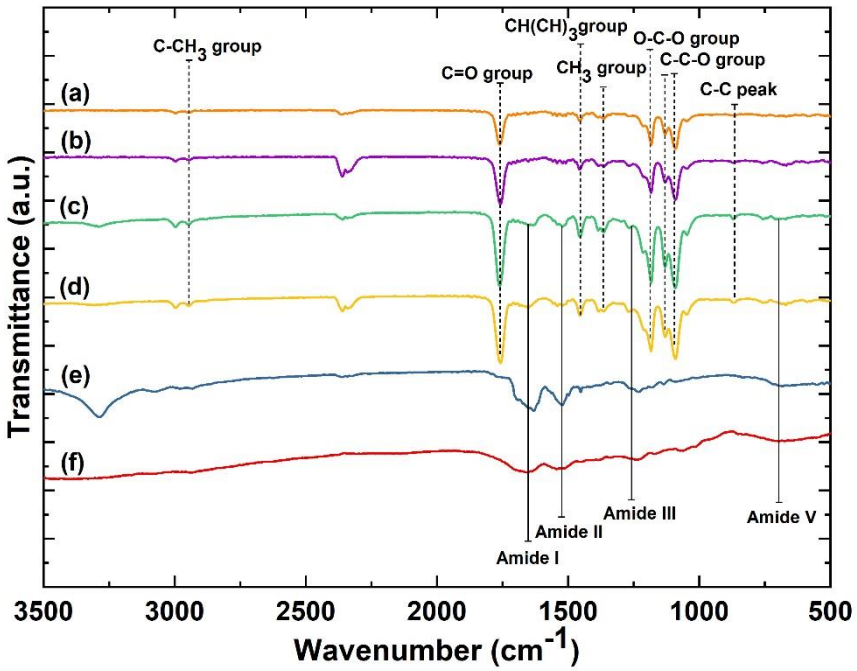

Figure 2 FTIR spectra of nanofiber scaffolds: PLA (a), methanol-treated and (b) untreated, SF/PLA (50:50) (c), methanol-treated and (d) untreated, and SF (e), methanol-treated and (f) untreated

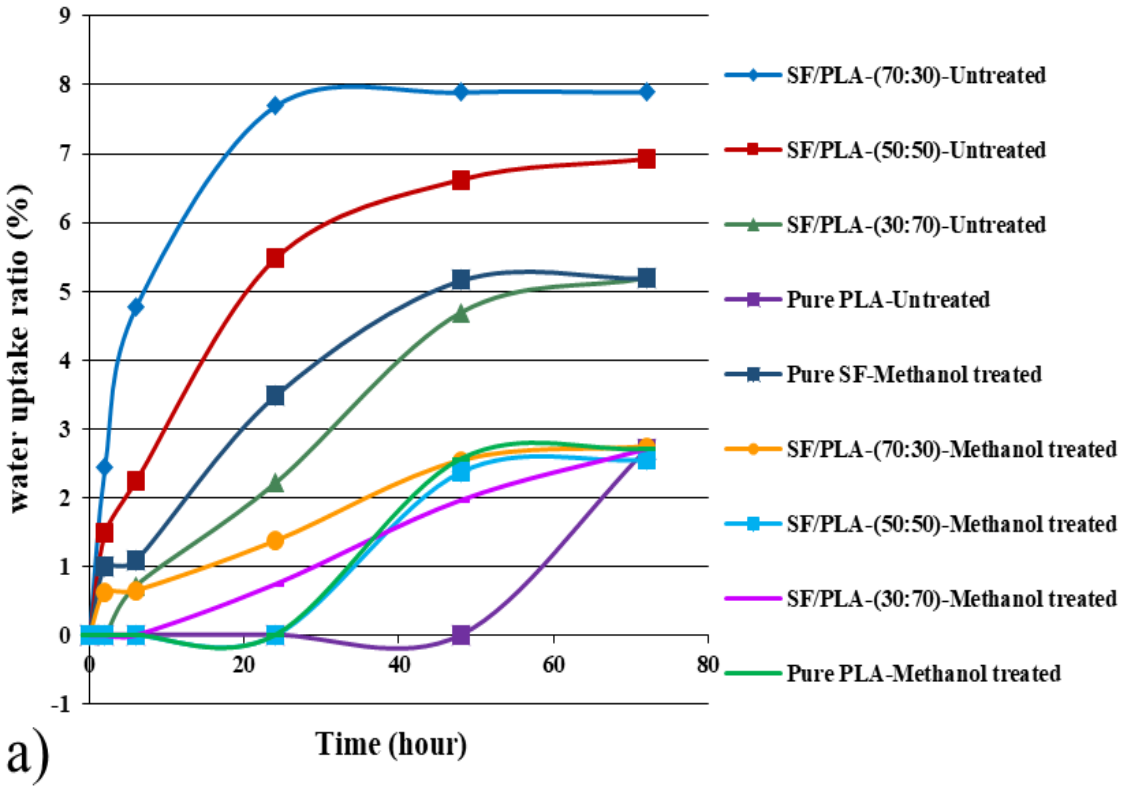

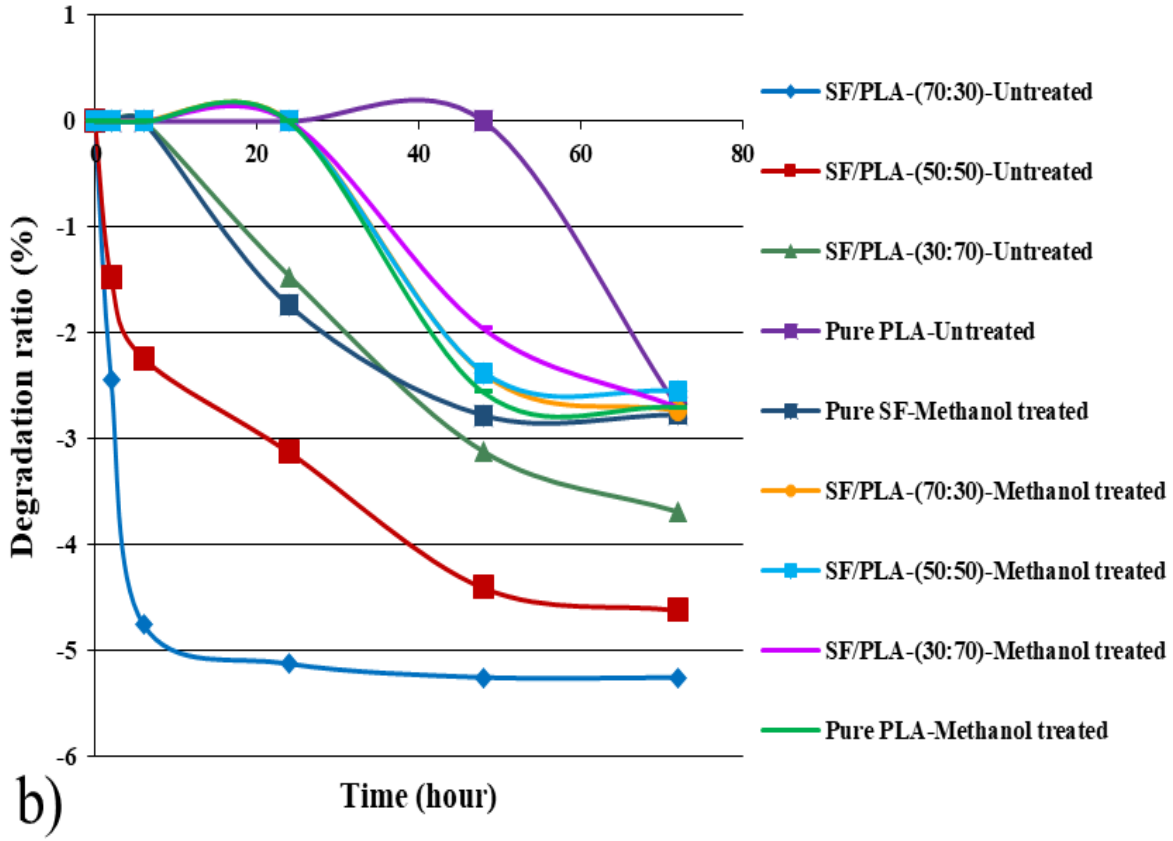

Figure 3 (a) Water absorption and (b) degradation of different nanofiber scaffolds. The pure, untreated SF scaffold was completely dissolved in PBS after one minute. (c) SEM pictures of nanofiber scaffolds with methanol treatment after 48 hours of degradation: (a) Pure SF and (c) Pure PLA (scale bar: 3 µm= 3000 nm)

In this work, the effect of methanol and the blending of two polymers with different hydrophilicity on degradation behaviors was investigated. All nanofibrous webs exhibited weight loss as a function of time (Figure 3(b)). Interestingly, SF/PLA nanocomposites degraded more than PLA. Water exposure caused fibroin nanofibers to dissolve, reducing scaffold mass.

Figure 3(c) shows the water absorption test results for methanol-treated fibroin and neat polylactic scaffolds after 48 h. The fibroin nanofibers demonstrated some degradation due to the weakness and crystallinity of the beta structure, while the polylactic scaffold appeared nearly intact.

Table 2 The water contact angles of all the untreated and methanol-treated nanofibers after 3 and 10 seconds (n=6)

Samples	Contact angle (degree) at 3 sec				
	SF	**SF/PLA-(70:30)**	**SF/PLA-(50:50)**	**SF/PLA-(30:70)**	**PLA**
Untreated	70.03±2.0374	86.24±1.62	101.88±1.205	124.24±0.155	144.02±0.439
Methanol treated	44.27±6.976	50.5±3.412	52.43±1.865	104.86±1/827	131.63±1.673
	Contact angle (degree) at 10 sec				
	SF	**SF/PLA-(70:30)**	**SF/PLA-(50:50)**	**SF/PLA-(30:70)**	**PLA**
Untreated	35.45±0.562	51.3±0.495	70.42±0.680	110.12±0.500	142.63±0.701
Methanol treated	43.18±5.93	49.48±2.94	51.4±1.44	104.78±1.26	131.61±1.503

Surface Wettability of Electrospun Nanofibrous Scaffolds

The contact angles of water on untreated and methanol-treated nanofibers were measured after 3 seconds (Table 2). SF nanofibers showed high hydrophilicity with a contact angle of 70.03°. PLA had a higher contact angle than SF due to hydrophobic groups. Increasing the PLA/SF mass ratio increased the water contact angle of nanofiber scaffolds from 70.03° to 144.02°, indicating a decrease in the wettability. Methanol treatment enhanced wettability and decreased the water contact angle. Table 2 indicates the change in the water droplet contact angle after 10 seconds. All untreated fibers, except pure polylactic acid, showed a decrease in the contact angle after 10 seconds as a result of the degradation of fibroin and the absorption of water. In contrast, methanol-treated fibers showed only slight changes in contact angle. The current study demonstrated that methanol treatment initially improved the fiber surface structure, water absorption, and hydrophobicity. However, the contact angle stabilized over time due to the non-biodegradability of the scaffold. Methanol-treated nanofibers were the best scaffold with a favorable water droplet contact angle and reduced degradation rates.

Mechanical Properties

The result of the methanol action and combination of polymers on nanofiber performance was measured in terms of the stress-strain curves, as presented in Table 3. The experiment was conducted in triplicate to ensure reproducibility. In the mechanical strength test, polylactic acid (PLA) exhibited greater strength compared to silk fibroin (SF). This increase in both stress and elongation is quantitatively supported by the measured values (Table 3). In contrast, in samples treated with methanol, an increase in strength was observed, attributed to the formation of β-sheet structures. However, this enhancement in strength was accompanied by a reduction in elongation, likely due to increased brittleness and fragility of the scaffolds.

Table 3 Mechanical properties of the nanofiber scaffolds before and after methanol treatment (n=3, *p-value < 0.05, rectangular samples with widths of 20 mm and 10 mm, and a thickness of 100 to 150 µm, F=50 N, speed of 10 mm/min.). In each column, differing letters denote statistically significant differences as determined by Duncan's multiple range test at the 5% significance level

	Max Load (gf)	Max Elongation (mm)	Work of rupture (cN/Tex)	Final Load (gf)	Max Stress (cN/Tex)	Final Stress (cN/Tex)	Final Extension (%)	Extension at max Load (%)
Untreated								
SF	12.92±1.1^{e}	0.94±0.06^{d}	1.34±0.147^{d}	4.62±0.88^{e}	116.23±9.38^{e}	41.83±7.85^{e}	3.30±0.53^{d}	2.55±0.45^{c}
SF/PLA-(70:30)	16.05±2.01^{de}	2.01±0.138^{bcd}	4.47±232^{d}	6.16±1.02^{de}	145.46±17.76^{de}	58.44±9.67^{de}	8.07±0.55^{bc}	3.09±0.24^{c}
SF/PLA-(50:50)	19.57±0.626^{d}	3.16±0.72^{bc}	15.59±5.38^{bcd}	7.97±0.278^{d}	186.66±9.37^{d}	78.95±4.3^{d}	12.63±2.91^{bc}	8.13±4.07^{bc}
SF/PLA-(30:70)	28.33±2.217^{c}	3.94±1.36^{b}	30.056±11.3^{b}	11.48±0.88^{c}	275.7±23.69^{c}	116.72±10.37^{c}	15.77±5.44^{b}	10.63±4.23^{b}
PLA	47.24±3.44^{a}	6.52±0.5^{a}	92.32±10.37^{a}	19.03±1.38^{a}	506.33±42.68^{a}	210.86±16.84^{a}	26.09±2.04^{a}	27.71±2.41^{a}
Methanol-treated								
SF	-	-	-	-	-	-	-	-
SF/PLA-(70:30)	20.12±1.45^{d}	1.05±0.11^{d}	4.03±1.14^{d}	8.27±0.51^{d}	181.46±12.83^{d}	75.75±4.89^{d}	4.21±0.48^{d}	2.77±0.21^{c}
SF/PLA-(50:50)	31.95±1.41^{c}	1.78±0.085^{cd}	11.23±0.64^{bcd}	13.11±0.63^{c}	293.46±11.93^{bc}	123.26±5.59^{c}	7.12±0.33^{cd}	4.64±0.56^{bc}
SF/PLA-(30:70)	38.13±1.89^{b}	2.09±0.064^{bcd}	1934±1.59^{bcd}	16.05±0.56^{b}	352.8±19.15^{b}	152.93±5.54^{b}	8.49±0.16^{bc}	5.45±0.51^{bc}
PLA	50.90±1.83^{a}	6.20±0.81^{a}	91.85±13.96^{a}	20.78±0.88^{a}	539.90±18.77^{a}	227.63±9.44^{a}	24.81±3.27^{a}	20.72±1.64^{a}

Assessment of Biocompatibility or Biological Effects

Microscopic Observation and Cell Count

Figure 4 (a) illustrates fibroblast cell counts on nanofibrous scaffolds from H&E staining at days 1, 3, and 7. The average cell count was based on twenty images. The largest increase occurred on day seven. Figure 4(b) highlights the best conditions on that day. Additionally, Figure 4(b) depicts the attachment of human fibroblasts on untreated and methanol-treated nanofiber surfaces, in comparison with the control sample, after 7 days. In general, untreated neat PLA nanofiber scaffolds were not conducive to cell proliferation. However, when these scaffolds were incorporated with SF, an increase in cell proliferation was observed. Meanwhile, the untreated neat SF nanofiber scaffold did not meet the standard for cellular growth. Fibroblasts spread widely after 2 to 4 hours, attaching and forming filopodia. After 24 h, they began to migrate and proliferate. Methanol treatment improved fibroblast attachment to nanofibers and enhanced proliferation. The SF/PLA (70:30) composite in the methanol-treated group favored cell growth (Figure 5-g).

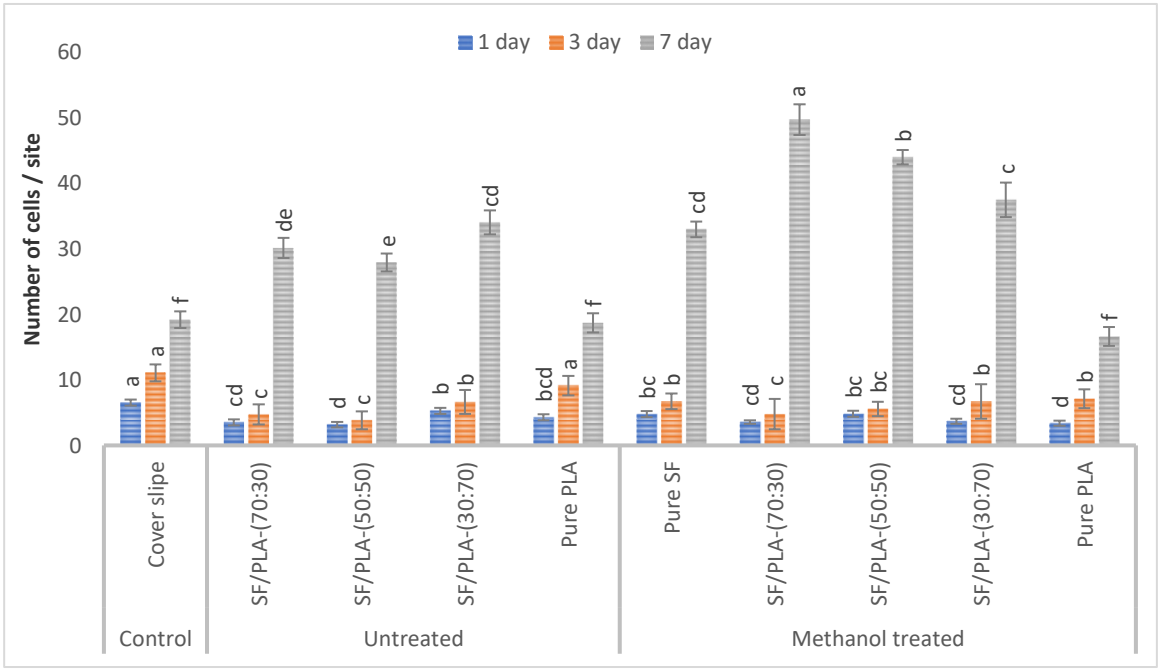

a)

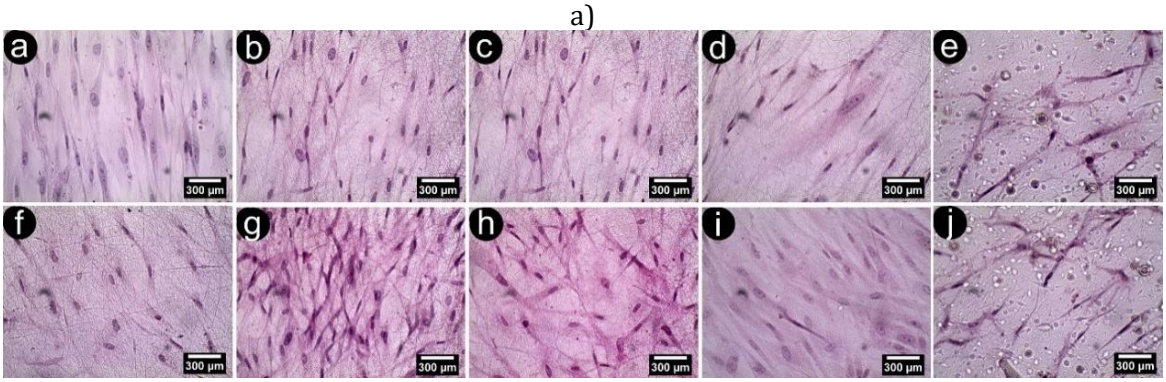

b)

Figure 4 (a). The cell counts of fibroblast cells cultured on nanofibrous scaffolds, as assessed through H&E staining images on days 1, 3, and 7 (n=20, *p-value < 0.05). Distinct English letters above each graph indicate statistically significant differences according to Duncan's multiple range test at the 5% significance levelb). The human fibroblasts adhered to different surfaces after 7 days of culture. Samples were stained with H&E: (a) Control sample, without methanol treatment: (b) SF/PLA-(70:30), (c) SF/PLA-(50:50), (d) SF/PLA-(30:70), (e) PLA; and with methanol treatment: (f) SF, (g) SF/PLA-(70:30), (h) SF/PLA-(50:50), (i) SF/PLA-(30:70), and (j) PLA (scale bar: 300 µm)

SEM analysis also showed good adhesion and spreading of human fibroblasts on the composite scaffolds (Figure 5(a)). Fibroblasts on the SF/PLA (70:30) composite showed more filopodia around nanofibers, indicating better attachment. In general, the results indicate that human fibroblasts attached well and expressed a normal phenotype. In Figure 5 f–j, the cells cultured for 3 days showed a larger body and were denser than the methanol-treated group, and the fibroblast connections began to form.

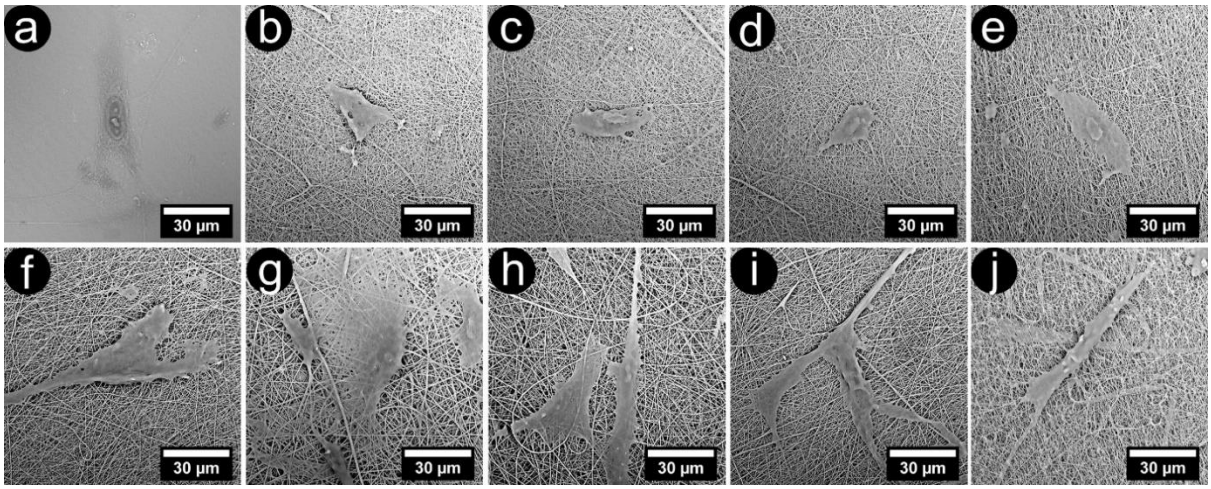

a)

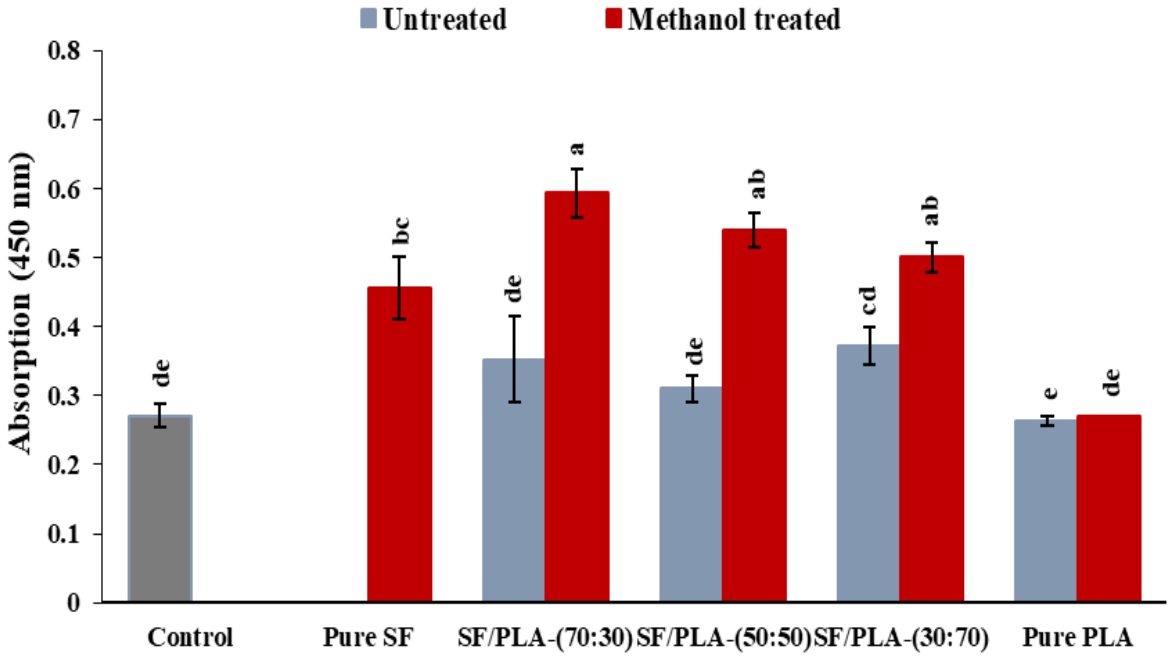

b)

Figure 5 (a). SEM pictures of the human fibroblasts cultured on the (a) control sample, without methanol treatment: (b) SF/PLA-(70:30), (c) SF/PLA-(50:50), (d) SF/PLA-(30:70), (e) PLA; and with methanol treatment: (f) SF, (g) SF/PLA-(70:30), (h) SF/PLA-(50:50), (i) SF/PLA-(30:70), and (j) PLA after 3 days of culture (scale bar: 30 µm= 30000nm). (b). MTT results of human fibroblast growth on various types of SF/PLA scaffolds after 7 days (*p-value < 0.05). Distinct English letters above each graph indicate statistically significant differences according to Duncan's multiple range test at the 5% significance level

MTT Assay

Figure 5 (b) demonstrates that all nanofiber scaffolds promoted human fibroblast growth and were not cytotoxic. After 7 days, a notable difference in cell growth was observed between the scaffolds with varying ratios and the control. Methanol-treated SF/PLA (70:30) nanofibers exhibited the highest cell proliferation rate. Cell proliferation on SF/PLA scaffolds was markedly greater than in the controls ($p < 0.05$), proving that the composition of the scaffold improved growth. The MTT

assay presented a considerable rise in the growth of cells on the methanol-treated SF/PLA scaffolds in varying ratios ($p < 0.05$).

In Vivo Wound Healing

In this study, two excision wounds were made on animals and treated with nanofibrous scaffolds and controls to enhance healing. Wound size was measured on days 0, 9, and 18. Figure 6 (a) and Tables 4 and 5 show that SF/PLA-(50:50) nanofibrous scaffolds had significantly higher wound healing rates than other treatments. By day 9, these scaffolds achieved a wound closure rate of 63.1 ± 0.52^{c} %. On day 18, the animals achieved a 100±0% closure rate, earlier than in other treatments. The wound closure rate was higher in SF/PLA-(50:50) nanofibrous scaffolds compared with other scaffolds; thus, this scaffold showed an efficient improvement in the initial stage of wound healing (p-value < 0.05). Histopathological results are shown in Table 5 and Figure 6 (b). Scaffolds with SF/PLA-(30:70) and SF/PLA-(50:50) showed improved skin healing histologically. The SF/PLA-(50:50) scaffold produced more skin structure than the SF/PLA-(30:70) scaffold, as shown in Figure 6 (b).

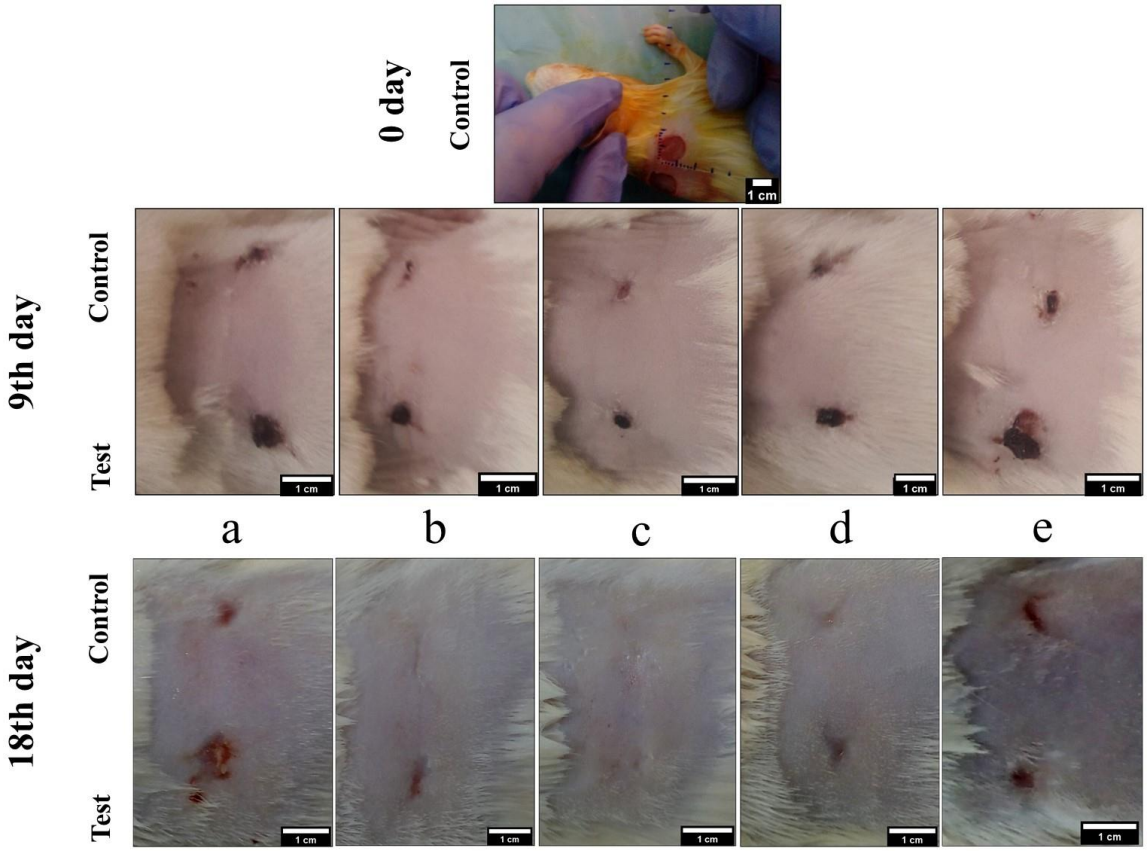

a)

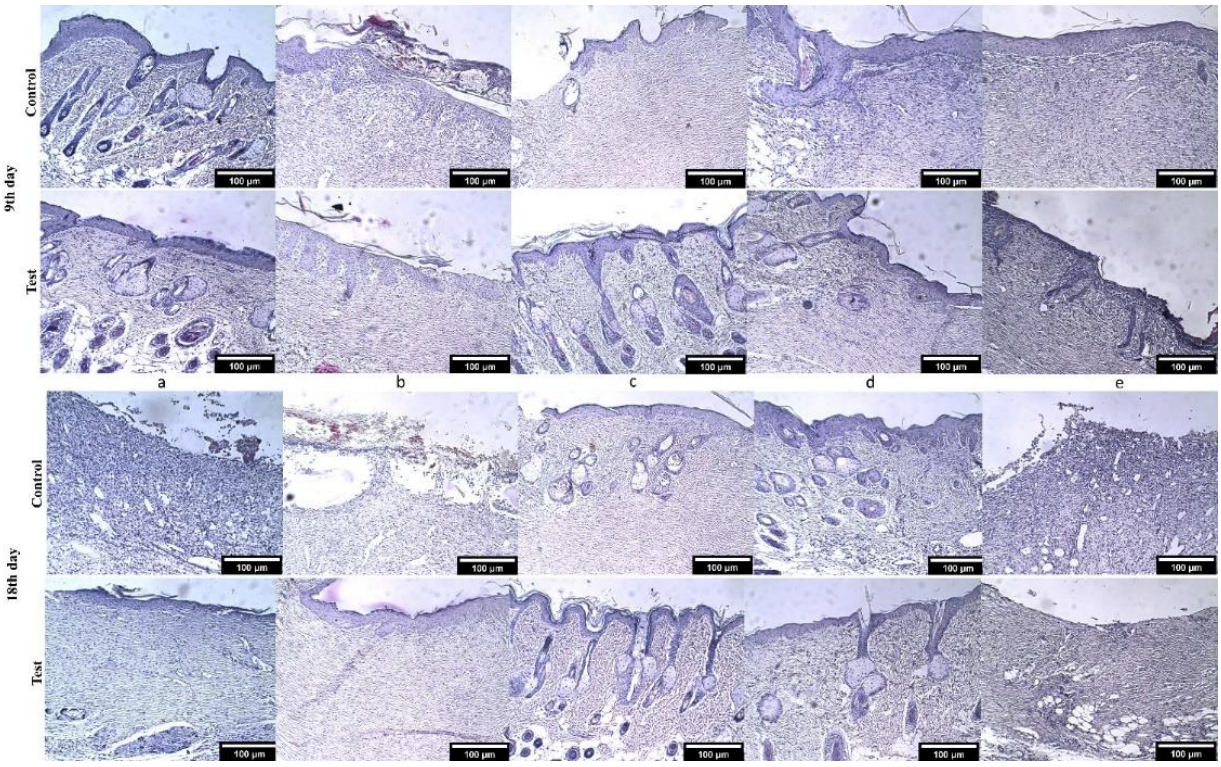

b)

Figure 6 (a). The macroscopic appearance of wounds was compared in 9 and 18 days of the experiment: a. SF (9 or 18 days), b. SF/PLA70/30 (9 or 18 days), c. SF/PLA50/50 (9 or 18 days), d. SF/PLA30/70 (9 or 18 days), and e. PLA (9 or 18 days). (b). The histo-pathological evaluation of wounds was compared in 9 and 18 days of the experiment: a. SF (9 or 18 days), b. SF/PLA70/30 (9 or 18 days), c. SF/PLA50/50 (9 or 18 days), d. SF/PLA30/70 (9 or 18 days), and e. PLA (9 or 18 days)

Table 4 Wound closure (%) over 18 days for each treatment group (n=3, *p-value < 0.05). In each column, differing letters denote statistically significant differences as determined by Duncan's multiple range test at the 5% significance level

Substrate	**Wound closure (%)**	
	9 (Days)	**18 (Days)**
Control	65.23±2.08^{cd}	65.96±4.44^{cd}
SF	54±0.25^{f}	66.93±0.26^{c}
SF/PLA-(70:30)	59.3±0.4^{e}	78.13±0.31^{b}
SF/PLA-(50:50)	63.1±0.52^{cde}	100±0^{a}
SF/PLA-(30:70)	62.1±0.34^{de}	80.36±0.46^{b}
PLA	54.3±0.26^{f}	65.913±70.26^{cd}

Table 5 The histopathological evaluation of wounds was compared at 9 and 18 days of the experiment

Scaffolds	Day 9 Test (Left side)	Control (Right side)	Day 18 Test (Left side)	Control (Right side)
PLA	1) Presence of a blood cell, trapped in the wound area 3) New blood vessels 4) proliferation of fibroblasts 5) Formation of granulation tissue	1) Re-epithelialisation and formation of a thick layer of epidermis 2) New blood vessels 3) Formation of dermis 4) No formation of epidermis ridge and dermal papilla 5) No formation of skin appendages 6) Formation of a thin horny layer	1) less blood cell infiltration compared test, gay 9 2) New blood vessels 3) proliferation of fibroblasts 4) Formation of granulation tissue 5) Formation of hypodermis with sweat glands	1) Re-epithelialisation 2) Formation of epidermis and dermis 3) New blood vessels 4) Epidermis ridge and dermal papilla
SF	1) Presence of a blood cell, trapped in the wounded area 3) New blood vessels 4) proliferation of fibroblasts 5) Formation of granulation tissue	1) Re-epithelialisation 2) Formation of dermis and epidermis 2) Epidermis ridge and dermal papilla 3) Development of skin appendages such as sebaceous glands, sweat glands, and hair follicles. 4) A thin horny layer	1) Re-epithelialisation and formation of a thin and irregular layer of epidermis 2) New blood vessels 3) Formation of dermis 4) No formation of epidermis ridge and dermal papilla 5) No formation of skin appendages 6) Formation of a thin horny layer	1) Re-epithelialisation 2) Formation of dermis and epidermis 2) Development of skin appendages such as sebaceous glands, sweat glands, and hair follicles.3) A thin horny layer
SF/PLA (30:70)	1) Re-epithelialisation 2) Formation of dermis and epidermis 2) Epidermis ridge and dermal papilla 3) Development of skin appendages such as sebaceous	1) Re-epithelialisation 2) Formation of dermis and epidermis 2) Fewer epidermis ridge and dermal papillae 3) Formation of hair follicles	1) Re-epithelialisation 2) Formation of dermis and epidermis 2) Epidermis ridge and dermal papilla 3) Development of skin appendages such as sebaceous	1) Re-epithelialisation 2) Formation of dermis and epidermis 2) Epidermis ridge and dermal papilla 3) Less formation of

Scaffolds	Day 9 Test (Left side)	Control (Right side)	Day 18 Test (Left side)	Control (Right side)
	glands, sweat glands, and hair follicles. 4) A thin horny layer	4) A thin horny layer **5)** Formation of hypodermis with sweat glands	glands, sweat glands, and hair follicles.4) A thin horny layer	sebaceous and hair follicles, compared to the control 4) A thin horny layer
SF/PLA (50:50)	1) Re-epithelialisation and development of a thin and irregular epidermal layer 2) Formation of dermis and epidermis 3) No epidermis ridge and dermal papilla 4) Development of skin appendages such as sebaceous glands, sweat glands, and hair follicles.	1) Re-epithelialisation 2) Development of a thick and irregular epidermal layer 2) Formation of epidermal ridge and dermal papilla 3) No formation of skin appendages 4) Formation of a thin horny layer	1) Re-epithelialisation 2) development of a thick and irregular epidermal layer. 3) Formation of epidermal ridge and dermal papilla 4) Complete ddevelopment of skin appendages such as sebaceous glands, sweat glands, and hair follicles .5) Formation of a thin horny layer 6) New blood vessels	1) Re-epithelialisation 2) development of dermis and epidermis 3) Epidermis ridge and dermal papilla 4) Less development of skin appendages such as sebaceous glands, sweat glands, and hair follicles., compared to control 5) A thin horny layer
SF/PLA (70:30)	1) Presence of white and red blood cells, trapped in the wounded area 3) New blood vessels 4) proliferation of fibroblasts 5) Formation of granulation tissue	1) Re-epithelialisation and formation of a thick and irregular layer of epidermis 2) Formation of epidermal ridge and dermal papilla 3) No formation of skin appendices 4) Formation of a thick horny layer	1) Re-epithelialisation and formation of a thick and irregular layer of epidermis 2) Formation of epidermal ridge and dermal papilla 3) No formation of skin appendices	1) Re-epithelialisation 2) Formation of dermis and epidermis 2) Epidermis ridge and dermal papilla 3) A thin horny layer

Discussion

In tissue engineering, the characteristics of scaffolds are crucial for supporting cell growth and differentiation [3,13,14], including mechanical strength, compatibility with

biological systems, and the ability to biodegrade [13,14]. Several methods for fabricating TE scaffolds are solvent casting, freeze drying, phase separation, fiber bonding, and electrospinning [13]. Electrospinning is prominent due to its effectiveness in rapidly fabricating scaffolds and enhancing properties such as morphology, porosity, pore size, and fiber size by simply adjusting the parameters [3,5]. Electrospun nanofibers mimic the natural ECM, featuring continuous fibers with high surface area and porosity, and varying pore sizes [3]. This work demonstrates that the concentration of the electrospun solution and the methanol treatment affect the nanofiber structure. When a higher content of PLA is used, the mean diameter of the nanofibers improves. Additionally, the SF contains charged functional groups, which, when exposed to an acidic solution, produce ions that decrease the mean diameter of the nanofibers during spinning. PLA has no surface functional groups; that is, it does not release charged ions, which have been reported to result in larger fiber diameters [9]. When pure SF and SF/PLA nanofibers were immersed in methanol, hydrogen bonds with hydrophilic proteins decreased the intermolecular forces between them, and the nanofibers swelled, increasing their diameter. On the other hand, virgin PLA nanofibers did not show any significant changes, possibly due to their hydrophobic nature and structural stability [15]. Larger fiber diameters in electrospinning reduce nanofiber pore size [16]. These pores form a porous structure essential for nutrient and gas exchange, vital for cell proliferation and tissue regeneration [9]. The study confirms that methanol treatment of SF/PLA nanofiber scaffolds leads to a decrease in pore size. It focuses solely on the chemical treatment effects, excluding variations stemming from the electrospinning process. Securing and methanol treatment of fibers significantly reduce the pore size while increasing the fiber diameter, which is in contrast to some researchers and thus represents the first link between the larger nanofiber diameter and smaller pore size. A slight increase in the polylactic pores exposed to methanol has been recorded due to the possible degradation of the artificial polymer. FTIR analysis of the nanofiber structure revealed characteristic bands for PLA and fibroin. Untreated fibroin nanofibers showed absorption bands assigned to amide vibrations, which proved the formation of composite nanofibers from the SF and PLA blend. Methanol treatment slightly influenced the crystallinity of the nanofibers, especially concerning fibroin. Methanol treatment converted silk fibroin's structure from α-helix/random coil to β-sheet [8]. Alternatively, Sato *et al.* did not notice a chemical structure modification of PLA films in the cases of being immersed in solvents [17]. He *et al.* found that SF/PLA composite nanofibers showed overlapping absorption bands of the two components in the FTIR spectrum [18]. Methanol treatment of PLA/SF blend scaffolds shifted amide II intensity from 1538 to 1516 cm^{-1}, which is in agreement with our observation for untreated PLA/SF blend and SF powder [19]. Physicochemical biomaterial surface factors influencing cellular activity include hydrophilicity, surface chemical groups, charge, topography, and roughness. The physical and chemical changes of scaffold surfaces can be achieved through adsorption or chemical alteration, respectively [20]. The hydrophilicity of the scaffold surface is very important for cellular adhesion, growth, migration, and viability [21]. The water contact angles were measured to assess the wettability of the nanofibrous scaffolds. SF nanofibers were highly hydrophilic, while PLA was hydrophobic. The water contact angle

decreased with an increase in the SF to PLA mass ratio [9]. Methanol treatment enhanced the wettability of the nanofiber surface. Measurement of water contact angle indicated that treated nanofibers have better hydrophilicity than untreated scaffolds. Capillary pressure on porous surfaces drives liquid inward, thus reducing the contact angle [22,23]. Adding hydrophilic polymers, such as SF, to PLA can increase the hydrophilicity of PLA [24]. The data of the present study also support this, as the blended nanofibers had better wettability [25]. For nanofiber scaffolds to be effective in skin tissue engineering and wound healing, they must absorb water, as this influences drug release and moisture retention. The water absorption of electrospun mats depends on porosity, surface area, and hydrophilicity [26]. Degradability is an important factor in the evaluation of tissue engineering scaffolds [26,27]. In aqueous conditions, fibroin nanofibers dissolve, and the weight of the scaffold decreases. The polar groups on SF nanofibers may increase their interaction with water and facilitate the degradation of fibroin [28].

SF degrades faster than PLA [25,28]. Our findings are in line with the water-resistant characteristics that allow SF/PLA blend nanofibers to dissolve slowly after implantation. Moreover, smaller fiber diameters in nanofiber scaffolds provide a higher surface-to-volume ratio, which accelerates hydrolytic degradation [29]. SF nanofibers in microfibers enhance water absorption [3,30]. The stable water uptake and low weight loss during biodegradation in the present study, result from the diversity in porosities and crystalline structures of silk fibroin [31].

The treated nanofibers with methanol exhibited less degradation than the untreated ones. This might be attributed to the presence of methanol, which slightly reduced degradation when methanol was added. The regular pattern of water absorption and the slight weight loss of the nanofiber scaffolds recorded during the biodegradation study may be ascribed to the unique crystalline structure of silk fibroin, as well as the different porosities presented [31]. This may be due to the enhanced β-sheet structure of fibroin from methanol treatment [8] .

The sructural integrity of the polymeric matrix is important in drug delivery [14, 32,33] and tissue engineering [14]. The untreated nanofibers degraded rapidly within a day, whereas the methanol-treated ones did not show any degradation even after 24 hours. The dissolution of fibroin nanofibers reduced surface chemical groups, which consequently limited surface interactions. Treatment with methanol preserved the groups, which retarded the scaffold degradation. The surfaces of nanofibers were modified to lower their degradability, and they were suitable for tissue engineering [34].

For biomedical applications, mechanical constancy of the electrospun nanofiber mesh is a significant parameter, as the structure must have enough strength to bear applied loads, cellular mechanical stresses, and forces due to movements of the body or other external environmental effects [35].

Other reports underscore the merits of SF/PLA blend nanofiber scaffolds, which possess greater thermal and mechanical stability compared to pure SF and PLA. The inclusion of SF improves cell adhesion and function [3,4,6].

These scaffolds can be used in drug delivery, biosensing, and as a framework for cell culture and tissue engineering. According to some researchers, an optimal tensile strength ranging from 0.8 to 18 MPa is recommended for effective dermal cell culture and wound dressing applications [36].

The fabricated nanofiber scaffolds possess suitable mechanical properties, making them appropriate for use as temporary support structures for transplanted cells and as wound dressings. Surface engineering of polymeric biomaterials is important for cell interaction. Scaffold surface hydrophilization can be achieved by either physical adsorption or chemical modification [20,30]. Chemical groups on the surface, such as hydroxyl, carbonyl, carboxyl, and amine, influence cell attachment [20].

The MTT assay showed that all nanofiber scaffolds supported human fibroblast growth and proliferation. Methanol-treated SF/PLA nanofibers promoted cell proliferation compared to control samples. Under light microscopy and SEM, human fibroblasts cultured on nanofiber scaffolds appeared to adhere well and spread, especially on the SF/PLA scaffolds. The treated nanofibers with methanol exhibited better hydrophilicity than the untreated ones. Previous studies have shown that human fibroblasts had better adhesion to amine and carboxyl surfaces compared to hydroxyl and hydrophobic methyl surfaces [37]. The blending of gelatin into the PLAGA surface may improve the cell-supporting matrix and mechanical properties of nanofiber scaffolds [38,39]. While the 70:30 SF/PLA scaffold demonstrated the highest fibroblast proliferation in vitro (Figure 5(b)), *in vivo* wound healing was significantly enhanced by the 50:50 and 30:70 scaffolds, particularly 50:50, which achieved 100% wound closure by day 18 (Figure 6 and Tables 4 and 5). This difference likely stems from mechanical strength and degradation behavior *in vivo*. The 50:50 scaffold may provide optimal mechanical support and a balanced degradation rate, favoring tissue regeneration. In contrast, 70:30 may degrade more quickly or have less structural integrity, which, despite supporting cell proliferation initially, could limit its effectiveness in the dynamic wound environment (Figure 3 and Table 3) [11,40].

This proves the beneficial effect of the scaffold on wound closure and epidermal repair. Shahverdi *et al.* (2014) showed that SF and PLGA [2:1] significantly improved wound healing in diabetic mice compared with controls [11]. SF, which is extracted from Bombyx mori silk, improves collagen synthesis and epithelial regeneration of skin wounds [11,30]. SF scaffolds also have excellent characteristics for wound dressing; for example, the permeability of dissolved oxygen, under wet conditions, is similar to healthy human skin. However, while the natural polymers scaffolds are hydrophilic and facilitate specific cellular interactions, they often possess poor tensile mechanical properties. In contrast, the hydrophobic characteristics of synthetic polymer scaffolds can impede cell seeding and lack adequate performance for cell recognition signals [11]. Synthetic biodegradable polymers, such as poly-L-lactic acid (PLA) and poly (lactic-co-glycolic acid) (PLGA), have been used for delivering stem cells to wounds [2]. For successful tissue regeneration, to function well in the performance of regenerative cells in wounds, the use of an appropriate cell scaffold compatible with the target tissue is essential [6,40]. Polylactic fibroin scaffolds are biocompatible, biodegradable, and non-toxic. They form an extracellular matrix that promotes the growth of stem cells through their nanofiber structure [4,6]. Stem cells at the scaffold site have been shown to enhance collagen formation, thereby supporting the repair of the epidermal layers of injured skin. This results in enhanced and faster wound healing.

Conclusion

This study investigated the morphology, structure, wettability, biodegradation, and cell compatibility of electrospun nanofibers from SF and PLA. The results indicated that the concentration of the suspension and methanol treatment significantly affected nanofiber morphology and crystallinity. Cell proliferation and adhesion on SF/PLA scaffolds were superior to those on SF and PLA scaffolds. In vivo studies in mice demonstrated that SF/PLA-50:50% promoted skin healing. Taken together, SF/PLA composite nanofibers hold great promise for tissue engineering and wound healing.

Acknowledgments

The authors would like to express their gratitude to the Stem Cell Biology Research Center (SCBRC), Yazd Reproductive Sciences Institute, Shahid Sadoughi University of Medical Sciences Yazd, Iran, for their valuable collaboration. Additionally, they would also like to extend their thanks to the collaborators of the Nano-Structured Coatings Institute at Yazd Payame Noor University of Iran for their support and cooperation.

Conflict of Interest

The authors declared that they had no conflict of interest.

Authors' Contributions

M.A.: performed experiments, analyzed data, and wrote the article; M.M.: Designed experiments, analyzed data, and rewrote the article ., H.N.: Designed experiments and edited the article, H.M.A: Designed experiments and edited articles, F.S.N.: Designed experiments, F.M.: performed in vivo experiments, and M.M: Help with *in vivo* experiment writing.

ORCID

Maede Afzali
https://orcid.org/0000-0002-8063-0648
Mahboubeh Mirhosseini
https://orcid.org/0000-0002-2010-5200
Habib Nikukar
https://orcid.org/0000-0001-9225-6019
Hosein Molla Hoseini
https://orcid.org/0009-0002-3461-0926
Fatemeh Sadeghian-Nodoushan
https://orcid.org/0000-0003-2767-7882
Fahime Mazaheri
https://orcid.org/0000-0002-2066-2656
Mojgan Moshrefi
https://orcid.org/0000-0002-6306-7881

References

[1]. Waghmare, V.S., Wadke, P.R., Dyawanapelly, S., Deshpande, A., Jain, R., Dandekar, P., Starch based nanofibrous scaffolds for wound healing applications. *Bioactive Materials*, **2018**, 3(3), 255-266.

[2]. Dash, B.C., Xu, Z., Lin, L., Koo, A., Ndon, S., Berthiaume, F., Dardik, A., Hsia, H., Stem cells and engineered scaffolds for regenerative wound healing. *Bioengineering*, **2018**, 5(1), 23.

[3]. Promnil, S., Ruksakulpiwat, Y., Ruksakulpiwat, C., Numpaisal, P. Effect of silk fibroin content on physical and mechanical properties of electrospun poly (lactic acid)/silk fibroin nanofibers for meniscus tissue engineering scaffold. *Journal of Physics: Conference Series*, **2022**, 2175(1), 012016.

[4]. Gu, H., Wang, F., Liu, H., Printon, K., Hu, X., Multifunctional silk fibroin–poly (l-lactic acid) porous nanofibers: Designing adjustable nanopores to control composite properties and biological responses. *Materials & Design*, **2022**, 222, 111053.

[5]. Taddei, P., Tozzi, S., Zuccheri, G., Martinotti, S., Ranzato, E., Chiono, V., Carmagnola, I., Tsukada, M., Intermolecular interactions between b. Mori silk fibroin and poly (l-lactic acid) in electrospun composite nanofibrous scaffolds. *Materials Science and Engineering: C*, **2017**, 70, 777-787.

[6]. Promnil, S., Ruksakulpiwat, C., Numpaisal, P., Ruksakulpiwat, Y., Electrospun poly (lactic acid) and silk fibroin based nanofibrous scaffold for meniscus tissue engineering. *Polymers*, **2022**, 14(12), 2435.

[7]. Liu, W., Li, Z., Zheng, L., Zhang, X., Liu, P., Yang, T., Han, B., Electrospun fibrous silk fibroin/poly (l-lactic acid) scaffold for cartilage tissue engineering. *Tissue Engineering and Regenerative Medicine*, **2016**, 13(5), 516-526.

[8]. Kaewpirom, S., Boonsang, S., Influence of alcohol treatments on properties of silk-fibroin-based films for highly optically transparent coating applications. *RSC advances*, **2020**, 10(27), 15913-15923.

[9]. Zhang, K., Wang, H., Huang, C., Su, Y., Mo, X., Ikada, Y., Fabrication of silk fibroin blended p (lla-cl) nanofibrous scaffolds for tissue engineering. *Journal of Biomedical Materials Research Part A: An Official Journal of The Society for Biomaterials, The Japanese Society for Biomaterials, and The Australian Society for Biomaterials and the Korean Society for Biomaterials*, **2010**, 93(3), 984-993.

[10]. Zhu, M., Gu, J., He, L., Mahar, F.K., Kim, I., Wei, K., Fabrication and osteoblastic adhesion behavior of regenerated silk fibroin/plla nanofibrous scaffold by double syringe electrospinning. *Fibers and Polymers*, **2019**, 20(9), 1850-1856.

[11]. Shahverdi, S., Hajimiri, M., Esfandiari, M.A., Larijani, B., Atyabi, F., Rajabiani, A., Dehpour, A.R., Gharehaghaji, A.A., Dinarvand, R., Fabrication and structure analysis of poly (lactide-co-glycolic acid)/silk fibroin hybrid scaffold for wound dressing applications. *International Journal of Pharmaceutics*, **2014**, 473(1-2), 345-355.

[12]. Qu, J., Wang, L., Hu, Y., Wang, L., You, R., Li, M., Preparation of silk fibroin microspheres and its cytocompatibility. **2013**.

[13]. Salemian, M., Jalali, H., Nabiuni, M., Mohseni, K.H., Evaluating the effect of 3d printed polycaprolactone-boric acid scaffold on proliferation and bone differentiation of human bone marrow mesenchymal stem cells. *International Journal of Advanced Biological and Biomedical Research*, **2024**, 12, 248.

[14]. Jahanbani, Y., Davaran, S., Yousefi, M., Roshangar, L., Bastani, P., Kadkhoda, J., Fabrication and characterization of col/pva nanofiber scaffolds for soft tissue engineering. *Chemical Methodologies*, **2024**, 8(5), 386-400.

[15]. Gui-Bo, Y., You-Zhu, Z., Shu-Dong, W., De-Bing, S., Zhi-Hui, D., Wei-Guo, F., Study of the electrospun pla/silk fibroin-gelatin composite nanofibrous scaffold for tissue engineering. *Journal of Biomedical Materials Research Part A: An Official Journal of The Society for Biomaterials, The Japanese Society for Biomaterials, and The Australian Society for Biomaterials and the Korean Society for Biomaterials*, **2010**, 93(1), 158-163.

[16]. Megelski, S., Stephens, J.S., Chase, D.B., Rabolt, J.F., Micro-and nanostructured surface morphology on electrospun polymer fibers. *Macromolecules*, **2002**, 35(22), 8456-8466.

[17]. Sato, S., Gondo, D., Wada, T., Kanehashi, S., Nagai, K., Effects of various liquid organic solvents on solvent-induced crystallization of amorphous poly (lactic acid) film. *Journal of Applied Polymer Science*, **2013**, 129(3), 1607-1617.

[18]. He, J., Qin, Y., Cui, S., Gao, Y., Wang, S., Structure and properties of novel electrospun tussah silk fibroin/poly (lactic acid) composite nanofibers. *Journal of Materials Science*, **2011**, 46(9), 2938-2946.

[19]. Li, L., Li, H., Qian, Y., Li, X., Singh, G.K., Zhong, L., Liu, W., Lv, Y., Cai, K., Yang, L., Electrospun poly (ε-caprolactone)/silk fibroin core-sheath nanofibers and their potential applications in tissue engineering and drug release. *International journal of biological macromolecules*, **2011**, 49(2), 223-232.

[20]. Vladkova, T.G., Surface engineered polymeric biomaterials with improved biocontact properties. *International Journal of Polymer Science*, **2010**, 2010(1), 296094.

[21]. Radakovic, D., Reboredo, J., Helm, M., Weigel, T., Schürlein, S., Kupczyk, E., Leyh, R.G., Walles, H., Hansmann, J., A multilayered electrospun graft as vascular access for hemodialysis. *Plos One*, **2017**, 12(10), e0185916.

[22]. Patnaik, A., Rengasamy, R., Kothari, V., Ghosh, A., 2. Wetting. *Textile Progress*, **2006**, 38(1).

[23]. Ravandi, S.A.H., Sanatgar, R.H., Dabirian, F., Wicking phenomenon in nanofiber-coated filament yarns. *Journal of Engineered Fibers and Fabrics*, **2013**, 8(3), 155892501300800302.

[24]. Hendrick, E., Frey, M., Increasing surface hydrophilicity in poly (lactic acid) electrospun fibers by addition of pla-b-peg co-polymers. *Journal of Engineered Fibers and Fabrics*, **2014**, 9(2), 155892501400900219.

[25]. Ravichandran, R., Venugopal, J.R., Sundarrajan, S., Mukherjee, S., Ramakrishna, S., Precipitation of nanohydroxyapatite on plla/pblg/collagen nanofibrous structures for the differentiation of adipose derived stem cells to osteogenic lineage. *Biomaterials*, **2012**, 33(3), 846-855.

[26]. Jiang, Z., Zheng, Z., Yu, S., Gao, Y., Ma, J., Huang, L., Yang, L., Nanofiber scaffolds as drug delivery systems promoting wound healing. *Pharmaceutics*, **2023**, 15(7), 1829.

[27]. John, J.V., McCarthy, A., Karan, A., Xie, J., Electrospun nanofibers for wound management. *ChemNanoMat*, **2022**, 8(7), e202100349.

[28]. Wolfe, P., Sell, S., Ericksen, J., Simpson, D., Bowlin, G., The creation of electrospun nanofibers from platelet rich plasma. *Journal of Tissue Science and Engineering*, **2011**, 2(2), 2819-2828.

[29]. Chen, V.J., Ma, P.X., The effect of surface area on the degradation rate of nano-fibrous poly (l-lactic acid) foams. *Biomaterials*, **2006**, 27(20), 3708-3715.

[30]. Zhu, H., Feng, X., Zhang, H., Guo, Y., Zhang, J., Chen, J., Structural characteristics and properties of silk fibroin/poly (lactic acid) blend films. *Journal of Biomaterials Science, Polymer Edition*, **2009**, 20(9), 1259-1274.

[31]. Yan, L.-P., Oliveira, J.M., Oliveira, A.L., Caridade, S.G., Mano, J.F., Reis, R.L., Macro/microporous silk fibroin scaffolds with potential for articular cartilage and meniscus tissue engineering applications. *Acta Biomaterialia*, **2012**, 8(1), 289-301.

[32]. Bahadorloo, Z., Piravar, Z., Sabaghzadeh, J., The effect of low-level laser therapy on differentiation ability of human adipocyte-derived stem cells to keratinocytes. *International Journal of Advanced Biological and Biomedical Research*, **2023**, 11(2), 82-93.

[33]. Al-Ani, I., Suryawanshi, R., Daoud, E., Dayyih, W., Lk, rb patnool, t. Begum, hs dol, mb duza, nanoparticle-mediated delivery of therapeutics for blood cancer treatment: A review of recent developments. *Journal of Chemical Reviews*, **2025**, 7(3), 331-357.

[34]. Adeli-Sardou, M., Yaghoobi, M.M., Torkzadeh-Mahani, M., Dodel, M., Controlled release of lawsone from polycaprolactone/gelatin electrospun nano fibers for skin tissue regeneration. *International Journal of Biological Macromolecules*, **2019**, 124, 478-491.

[35]. Ranjbar-Mohammadi, M., Bahrami, S.H., Development of nanofibrous scaffolds containing gum tragacanth/poly (ε-caprolactone) for application as skin

scaffolds. *Materials Science and Engineering: C*, **2015**, 48, 71-79.
[36]. Gomes, S.R., Rodrigues, G., Martins, G.G., Roberto, M.A., Mafra, M., Henriques, C., Silva, J.C., In vitro and in vivo evaluation of electrospun nanofibers of pcl, chitosan and gelatin: A comparative study. *Materials Science and Engineering: C*, **2015**, 46, 348-358.
[37]. Faucheux, N., Schweiss, R., Lützow, K., Werner, C., Groth, T., Self-assembled monolayers with different terminating groups as model substrates for cell adhesion studies. *Biomaterials*, **2004**, 25(14), 2721-2730.
[38]. Kim, H.W., Yu, H.S., Lee, H.H., Nanofibrous matrices of poly (lactic acid) and gelatin polymeric blends for the improvement of cellular responses. *Journal of Biomedical Materials Research Part A: An Official Journal of The Society for Biomaterials, The Japanese Society for Biomaterials, and The Australian Society for Biomaterials and the Korean Society for Biomaterials*, **2008**, 87(1), 25-32.
[39]. Gu, S.Y., Wang, Z.M., Ren, J., Zhang, C.Y., Electrospinning of gelatin and gelatin/poly (l-lactide) blend and its characteristics for wound dressing. *Materials Science and Engineering: C*, **2009**, 29(6), 1822-1828.
[40]. Krishani, M., Shin, W.Y., Suhaimi, H., Sambudi, N.S., Development of scaffolds from bio-based natural materials for tissue regeneration applications: A review. *Gels*, **2023**, 9(2), 100.

How to cite this article:
M. Afzali, Mahboubeh Mirhosseini, Habib Nikukar, Hosein Molla Hoseini, Fatemeh Sadeghian-Nodoushan, Fahime Mazaheri, Mojgan Moshrefi. Characterization and Performance Evaluation of Silk Fibroin/Polylactic Acid Composite Nanofiber Scaffolds for Tissue Engineering and Wound Healing. *International Journal of Advanced Biological and Biomedical Research*, 2026, 14(1), 48-71.
DOI: https://doi.org/10.48309/ijabbr.2026.2063133.1619
Link: https://www.ijabbr.com/article_729164.html

Copyright © 2026 by authors and SPC (Sami Publishing Company) + is an open access article distributed under the Creative Commons Attribution License(CC BY) license (https://creativecommons.org/licenses/by/4.0/), which permits unrestricted use, distribution, and reproduction in any medium, provided the original work is properly cited.